Faster Form of Electron Magnetic Reconnection with a Finite Length X-Line

P. S. Pyakurel, M. A. Shay, J. F. Drake, T. D. Phan, P. A. Cassak, and J. L. Verniero

Phys. Rev. Lett. **127**, 155101 — Published 7 October 2021

DOI: 10.1103/PhysRevLett.127.155101

A faster form of electron magnetic reconnection with a finite length X-line

P. S. Pyakurel[1],* M.A. Shay[2], J.F. Drake[3], T.D. Phan[1], P.A. Cassak[4], and J.L. Verniero[1]
[1]*Space Sciences Laboratory, University of California, Berkeley, CA 94720, USA*
[2]*University of Delaware, Newark, DE, 19716, USA*
[3]*Department of Physics and the Institute for Physical Science and Technology, University of Maryland, College Park, MD 20742, USA and*
[4]*Department of Physics and Astronomy and Center for KINETIC Plasma Physics, West Virginia University, Morgantown, WV 26506, USA*
(Dated: September 10, 2021)

Observations in Earth's turbulent magnetosheath downstream of a quasi-parallel bow shock reveal a prevalence of electron-scale current sheets favorable for electron-only reconnection where ions are not coupled to the reconnecting magnetic fields. In small-scale turbulence, magnetic structures associated with intense current sheets are limited in all dimensions. And since the coupling of ions are constrained by a minimum length scale, the dynamics of electron reconnection is likely to be 3D. Here, both 2D and 3D kinetic particle-in-cell simulations are used to investigate electron-only reconnection, focusing on the reconnection rate and associated electron flows. A new form of 3D electron-only reconnection spontaneously develops where the magnetic X-line is localized in the out-of-plane (z) direction. The consequence is an enhancement of the reconnection rate compared with 2D, which results from differential mass flux out of the diffusion region along z, enabling a faster inflow velocity and thus a larger reconnection rate. This outflow along z is due to the magnetic tension force in z just as the conventional exhaust tension force, allowing particles to leave the diffusion region efficiently along z unlike 2D configuration.

Magnetic reconnection in current sheets converts magnetic energy into particle energy, an important process in many laboratory, space and astrophysical contexts [1]. It is the dominant mechanism by which solar wind energy enters Earth's magnetosphere [2, 3]. Previous observational and theoretical studies have focused mainly on standard reconnection in large-scale current sheets, in which both ions and electrons are involved in the dynamics of this energy conversion process.

Recent observations of current sheets (CS) in Earth's highly turbulent magnetosheath region downstream of a quasi-parallel bow shock revealed a new form of reconnection involving only electrons, with no ion coupling [4]. In the electron-only reconnection events, the electron-scale reconnection CS was not embedded inside of an ion-scale CS as expected for a crossing of the electron diffusion region associated with standard ion-coupled reconnection [5–7]. Having wider CS at scales comparable to the ion inertial scale is not sufficient to induce ion coupling, as observations of Earth's bow shock have found electron-only reconnection with no ion response inside ion scale CS [8, 9].

Simulation have shown that ions become decoupled from reconnecting magnetic field when the length of the CS (in the outflow direction) is a few inertial lengths d_i [10] up to around ten d_i [11], depending on plasma conditions. Since the length scale size of turbulent magnetic structures in the magnetosheath can be quite small, exhibiting correlation scales on the order of 1-10 d_i [12, 13], electron-only reconnection may be the dominant form of reconnection in the turbulent magnetosheath and bow shock. Local kinetic simulations of Earth's bow shock find that electron-only reconnection is a frequent occurrence [14].

In collisionless turbulence, reconnection has been suggested to drive the energy dissipation at kinetic scales [15–17]. Below ion kinetic length scales, models suggest that the aspect ratio of turbulence eddies is governed by the balance of the eddies' turnover time with reconnection timescale mediated from electron tearing mode [18], which may facilitate a dominant form of magnetic energy release with further steepening of the energy spectrum [19]. The magnetic structures embedded in turbulence may be strongly 3D in nature, being limited in all directions. This fact and the prevalence of electron-only reconnection highlight the need for a kinetic study of 3D reconnection at electron scales.

In this study, we employ particle-in-cell (PIC) kinetic simulations of force-free CS with an out of reconnection plane (guide) magnetic field to study the 3D properties of electron reconnection. In the 3D simulation, multiple X-lines of finite extent spontaneously developed. Comparison with a 2D simulation reveals that $E_\parallel$ and hence the local reconnection rate is significantly larger in 3D. A control volume analysis of the 3D diffusion region shows a net mass flux in the out-of-plane direction (X-line direction) enabling a larger inflow velocity along the normal direction, leading to a faster reconnection rate.

We performed simulations in 2D and 3D using the PIC code P3D [20]. The normalizations are: magnetic fields and density to B_0 and n_0, time to $\Omega_{ce}^{-1} = m_e c/eB_0$, speeds to $c_{Ae} = B_0/\sqrt{4\pi m_e n_0}$, lengths to $d_e = c_{Ae}/\Omega_{ce}$, electric fields to $E_0 = c_{Ae}B_0/c$, where c is the speed of light and temperatures to $T_0 = m_e c_{Ae}^2$. A realistic mass ratio $m_i/m_e = 1836$, 10^3 particles-per-grid (ppg), speed of light $c/c_{Ae} = 2.33$ and uniform density

* pspyakurel@berkeley.edu

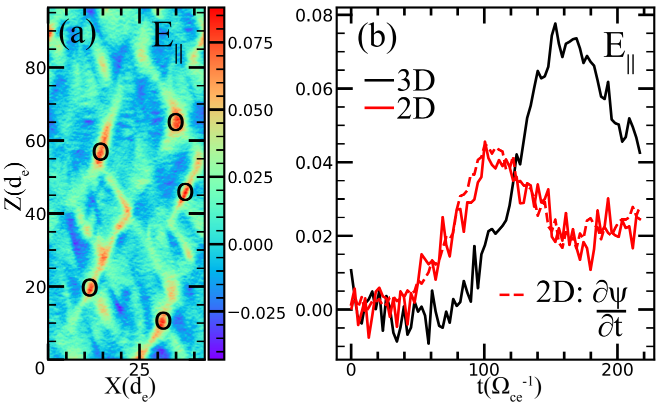

FIG. 1. (a) $E_\parallel$ over half the 3D simulation domain at $t = 152\Omega_{ce}^{-1}$ in the xz-plane at $y = 32.13$. The black circles are locations of X-lines associated with intense $E_\parallel$. The time evolution of one reconnection site located at $(x, y, z) = (14.14, 32.13, 55.27)$ is examined in (b). (b) Time evolution of peak $E_\parallel$ values are shown for 2D (red) and 3D (black) simulations. The solid curves show measurements of peak $E_\parallel$ around the X-line, while the dashed red line is calculated using the magnetic vector potential ψ.

$n = 1$ are chosen for both simulations. The ion and electron temperatures are $T_i = 2.7$ and $T_e = 0.27$, giving the Debye length $\lambda_{De} = \sqrt{2T_e}/c \simeq 0.31$ and the electron gyro-radius $\rho_e = \sqrt{2T_e} \simeq 0.73$. The 2D domain lengths $L_x \times L_y$ are $42.84d_e \times \; 42.84d_e$, while 3D $L_x \times L_y \times L_z$ are $42.84d_e \times \; 42.84d_e \times \; 192.77d_e$, with grid scale $\Delta \simeq 0.1674$, and time step $dt \simeq 0.06$. We use periodic boundary conditions in all directions and force-free initial conditions, with the initial magnetic fields given by $B_{\rm x} = \tanh[(y - 0.25\, L_{\rm y})/w_0] - \tanh[(y - 0.75 L_{\rm y})/w_0] - 1$ and $B_z = \sqrt{1 + B_{\rm g}^2 - B_{\rm x}^2}$, where $w_0 \simeq 1d_e$ is the half-width of the initial CS, $B_g = 1$ is the asymptotic guide field.

The initial CS consists solely of electron current with ions as a neutralizing background where magnetic reconnection onset is from particle noise.

In 3D, many finite-length X-lines grow throughout the simulation domain, indicated by intense $E_\parallel$ (black circles) in Fig. 1(a) at the center of one of the CS (xz-plane), while zero guide field simulation (not shown) didn't produce such localized $E_\parallel$. As they form, the X-lines propagate along the equilibrium electron current $(-\hat{z})$, as seen in previous fluid 3D simulations in the ion-coupled [21, 22] and electron-only [23, 24] regimes. However, in ion-scale current layers, simulations revealed that the X-line spreads in the current direction [25–27].

Before onset, we measure $E_\parallel$ at the location where the X-line initially forms and after the onset, we record the peak $E_\parallel$ in the vicinity of the X-line. In 3D, this vicinity is the region of a finite length X-line extended in z. In 2D, it is a spread of few grid points from the X-line. Reconnection onset is around $t \approx 46\Omega_{ce}^{-1}$ in 2D (Fig. 1(b)) for the X-line located at $x, y = 14.14, 32.13$ (Fig. 2(b)).

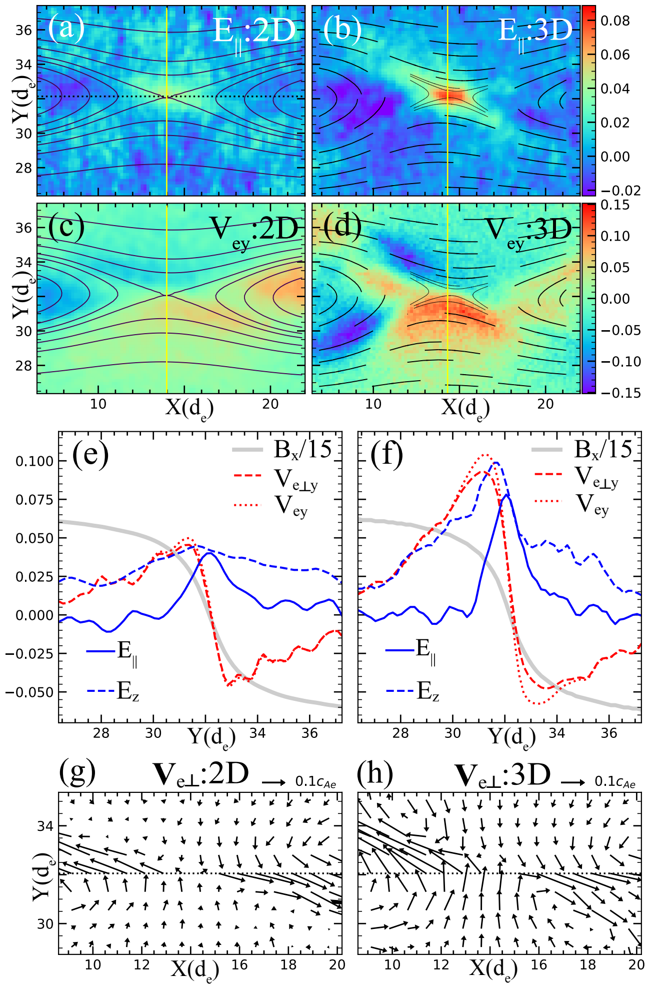

FIG. 2. 2D (left column) and 3D (right column at $z = 55.27$) results at $\sim 100\Omega_{ce}^{-1}$ and $\sim 152\Omega_{ce}^{-1}$, respectively, for the X-lines investigated in Fig. 1(b). The black contour lines in (a) & (c) are magnetic field lines while the black curves in (b) & (d) are short segments approximating projected magnetic field lines. The parallel electric field $E_\parallel$ is in (a) and (b). Panels (c) and (d) are inflows V_{ey}. In (e) and (f) are vertical cuts of B_x,V_{ey}, $V_{e\perp y}$, E_z and $E_\parallel$ along the vertical yellow lines in panels (a-d). The projection of electron flows on the xy-plane are the perpendicular flows $\mathbf{V}_{e\perp}$ in panel (g,h).

In 3D, the same method is applied except that onset occurs at $t \approx 75\Omega_{ce}^{-1}$ (Fig. 1(b)) for the X-line located at $x, y, z = 14.14, 32.13, 55.27$ (Fig. 1(a)). To remove fluctuations in $E_\parallel$ associated with reconfiguration of the initial CS, at each time the average of $E_\parallel$ is calculated at the center of the CS (a line in x in 2D and a $xz-$plane in 3D) then subtracted from the peak $E_\parallel$ to give the curve (black and red) in Fig. 1(b). As a cross-check of this method, the 2D reconnection rate is calculated in the more standard way as the difference in magnetic flux between the X-line and the O-line yielding results (dashed red line) similar to the method using direct $E_\parallel$ measurements. Note, numerical modelling studies have calculated reconnection rate in stationary 3D X-line using the change of magnetic flux [28–30].

In Fig. 1(b), a striking difference between the reconnection rate $E_\parallel$ in 2D and 3D is illustrated by a fast rise in the reconnection rate with a peak rate at $\sim 100\Omega_{ce}^{-1}$ and $\sim 152\Omega_{ce}^{-1}$, respectively. In 3D, the peak value of $E_\parallel$ is 7.76×10^{-2}, approximately twice the 2D peak value. 3D physics enhances the reconnection rate after the reconnection onset, which is not impacted when numerical factors such as grid spacing and ppg are changed.

To determine the cause of this enhanced reconnection rate, we study the two X-lines highlighted in Fig. 1(b) at the times of peak reconnection as illustrated in Fig. 2. Compared to 2D in Fig. 2(a), the measured $E_\parallel$ in 3D at the X-line is enhanced, shown by a region of dark red around the center in Fig. 2(b). The electron inflow velocities V_{ey} are also enhanced in 3D (Fig. 2(d)) compared to 2D inflow velocities (Fig. 2(c)). Figures 2(e)(2D) and (f)(3D) reveal peak values of V_{ey}, $V_{e\perp y}$ (vertical inflows perpendicular to the local magnetic fields), E_z and $E_\parallel$ in 3D are approximately twice as large as in 2D. In the same panels, the localized $E_\parallel$ structure is shown to be embedded within the CS as seen from the width associated with the reversal of the reconnecting magnetic field B_x. Both 2D and 3D show some localization of E_z but are not confined to the CS. The peak V_{ey} and $V_{e\perp y}$ are almost identical in the inflow region with speeds ∼0.1 in 3D (Fig. 2(f)) and ∼0.05 in 2D (Fig. 2(e)). The larger reconnection rate in 3D compared to 2D is because the inflowing velocity in 3D is enhanced.

The perpendicular flows $\mathbf{V}_{e\perp}$ (Figs. 2g(2D) and 2h(3D)) show a distinct inflow and outflow pattern of the electrons, indicating similar qualitative dynamics in 2D and 3D. In 3D, however, the velocity fields have more of a vortex-like pattern on either side of the primary perpendicular electron flows. Prominent structures are located at about $(11.14, 34.27)$ and $(17.14, 30.00)$ in Fig. 2(h). This structure extends in z, giving an almost-spiral electron flow, that are not as outstanding in 2D (Fig. 2(g)), making 3D electron outflows more spatially localized.

Additionally, 3D reconnection is non-uniform along z as seen in the $E_\parallel$ structure and $\mathbf{V}_{e\perp}$ flow pattern in Fig. 3. In Fig. 3(a), the outflowing plasma $\mathbf{V}_{e\perp}$ is ejected away from the slanted black dashed line. A dotted horizontal yellow line ($z = 55.27$) is drawn at the peak value of $E_\parallel$. For $z < 55.27$, the exhaust forms away from the dashed line following closely with the spread of $E_\parallel$. Similarly, the inflowing plasma in Fig. 3(b) is non-uniform along z. The $\mathbf{V}_{e\perp}$ points in $-\hat{y}$ above $y = 32.13$ and in $+\hat{y}$ below $y = 32.13$. The extension of the X-line is about $20d_e \sim 0.5d_i$ in $\hat{z}$ shown by the length of the red boxes in Fig. 3(a, b). In Fig. 3(c), cuts along the dashed black line in Fig. 3(a) reveal a net flow along z away from the peak in $E_\parallel$. This net flow is illustrated by the deviation of $\delta V_{ez} = V_{ez} + 0.55$ from the mean flow which is positive (negative) for z greater than (less than) the position of the peak in $E_\parallel$, where the mean flow of -0.55 is calculated by taking the average of V_{ez} at the midplane. This outflow along z is driven by magnetic tension just as the conventional outflow in 2D is driven by tension. Outside the red box, the z-component of magnetic tension force $\mathrm{B}^2(\mathbf{b}\cdot\nabla)\mathbf{b}$ (blue curve) points away from the underlying $E_\parallel$ structure, where $\mathbf{b} = \mathbf{B}/|\mathbf{B}|$. To sustain the net mass flux in z-direction, the 3D diffusion region develops larger inflow velocities and thus larger $E_\parallel$.

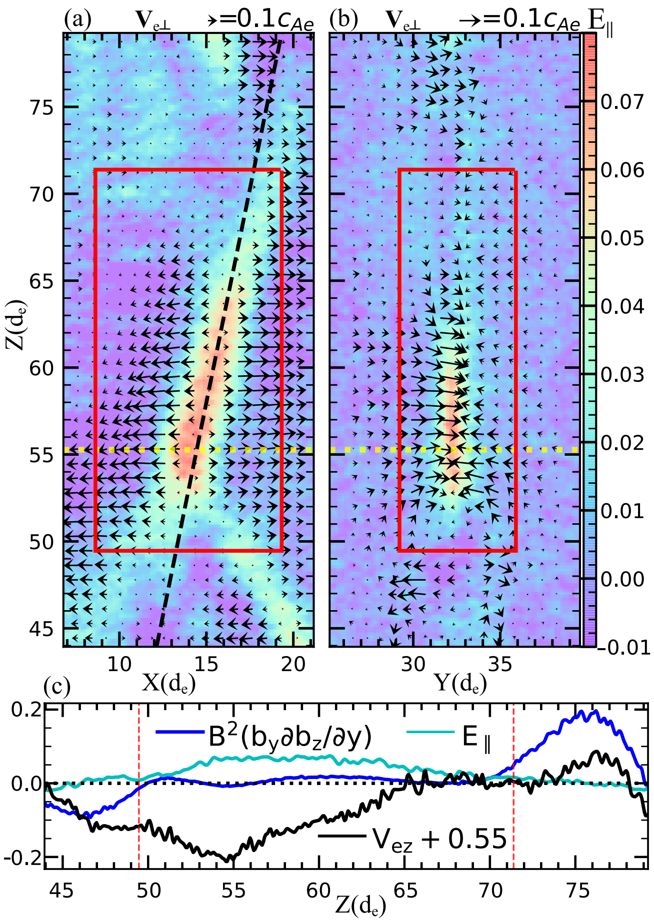

FIG. 3. (a) 3D electron flows $\mathbf{V}_{e\perp}$ at $y = 32.13$ in the xz-plane are diverging from the slanted dashed black line. (b) 3D electron flows $\mathbf{V}_{e\perp}$ converge inside the red boxed boundary in the yz-plane. The images of $E_\parallel$ in the (a) and (b) are overlaid, showing its finite and localized structure. (c) Cuts along the dashed black line in (a) are shown for V_{ez}, $E_\parallel$, and $B^2 b_y \partial b_z/\partial y$. The dashed vertical red lines denote z boundaries of the red boxes in (a,b).

The enhancement of $E_\parallel$ in 3D is linked to the increment of the speed of $V_{ey} \approx V_{e\perp y} \simeq V_{in}$ as shown in Fig. 2(f); this is because in the presence of the guide field at the X-line, $E_\parallel \simeq E_z$ and $E_z = V_{in}B_{up}/c$ since $\mathbf{E}\cdot\mathbf{B} = 0$ and $\mathbf{V}_\perp = c(\mathbf{E}\times\mathbf{B})/|\mathbf{B}|^2$ in the upstream region, where V_{in} is the upstream inflow speed and B_{up} is the upstream reconnecting magnetic field. We employ a 3D steady state control volume analysis [31] to the region of elevated $E_\parallel$ to probe how this increase of V_{in} is sustained in 3D versus 2D.

In Fig. 4, we choose a cuboid region enclosing the $E_\parallel$

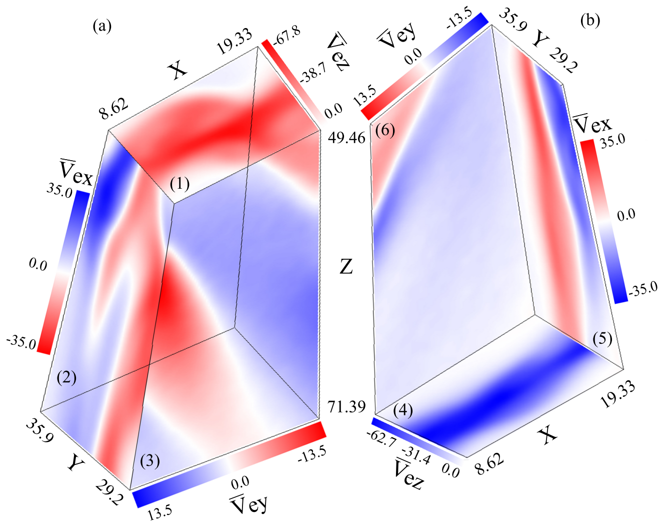

FIG. 4. 3D flow into and out of the diffusion region, where $\overline{\mathbf{V}}_e = \mathbf{V}_e \times 10^2$. Panels (a) and (b) show normal flow through each of the six faces of the diffusion region, which are numbered. For example, normal flow through face 1 at $z = 49.46$ is given by V_{ez}. The integrated mass flux (Equation 1) through each face is: $\Phi_{1,..,6} \approx 20.6, 1.5, -2.7, -17.9, 1.22, -2.91$.

structure shown by the red boxes in Fig. 3(a,b). Because there is little or no ion response, quasi-neutrality requires $\nabla \cdot \mathbf{V}_e \approx 0$. In discretized integral form, the mass flux through each face of the cuboid is given by

$$\Phi_j = \sum_{l,m} \left[\mathbf{V}_{e,j}(l,m) \cdot \hat{n}_j\right] \Delta^2, \tag{1}$$

where j is one of the six faces, $\hat{n}_j$ is the normal unit vector pointing out of the face, (l, m) indexes are the grid point locations on the surface of the face and Δ is the grid spacing. The calculated values for Φ_j are given in the caption of Fig. 4. The normal inflows into the diffusion box are shown in blue. For example, V_{ey} at $y = 35.9$ in face 6 mostly consists of a slanted blue strip. Similarly, the normal outflows are shown in red.

From Equation 1, the net mass flux in z is $\Phi_1 + \Phi_4 \approx 2.72$. In y, the sum of mass fluxes is $\Phi_3 + \Phi_6 \approx -5.61$. Finally, the sum of mass fluxes in x is $\Phi_2 + \Phi_5 \approx 2.72$. Thus, the net outward mass flux from the diffusion region along z is comparable to the sum of mass fluxes in x. The total mass flux (≈ 0.17) from Equation 1 is approximately an order of magnitude smaller than any direction's total mass flux contribution in Fig. 4, suggesting that the quasi-steady approximation is reasonable.

This implies that the modification to mass continuity in 3D induces the net outflow along z combined with the usual outflow in x to increase the inflow along y. This is consistent with the inflowing plasma flow V_{ey} being twice as fast as that measured in 2D. Such asymmetry was noted in an ion-coupled reconnection laboratory experiment [32] caused by an equilibrium non-uniformity. However, we find that the asymmetry develops spontaneously from the initially uniform 1D equilibrium.

Our results demonstrate a new form of electron-only reconnection in a 3D system in which the magnetic X-line is localized in the out-of-plane (z) direction. Using PIC simulations, we explored electron-only reconnection soon after its onset, comparing one finite length X-line in 3D with results from 2D. In both 2D and 3D, the parallel electric field is largest in the vicinity of the X-line and is equivalent to the local reconnection rate E_z. While both E_z and $E_\parallel$ are spatially localized near the X-line, $E_\parallel$ is more limited in extent than E_z. The 3D simulation exhibits both a larger $E_\parallel$ and inflow velocity; roughly twice their 2D counterparts. The driver of the larger inflow velocity in 3D is linked with the tension force in z, which ultimately drives a net outflow along z from the diffusion region. A control volume analysis of the diffusion region covering the $E_\parallel$ structure reveals that the net mass flux along z is equal to the total mass flux along x. This increased outward mass flux allows an inflow velocity twice what is present in 2D, leading to twice the reconnection rate.

We now compare the large electric fields in the 3D simulation with observations. In the turbulent magnetosheath, MMS observed large and coherent $E_\parallel$ of $\sim$ 7mV/m in a reconnecting CS [4]. In the context of electron-only reconnection, a comparison between this measured $E_\parallel$ and the simulation value can be made by normalizing it to inflowing plasma parameters given by $cE_\parallel/(c_{Ae,up}B_{up})$, where $c_{Ae,up}$ is the upstream electron Alfvén speed (using B_{up}). Normalized this way with $B_{up} = 5\,\mathrm{nT}$ and $n = 20\,\mathrm{cm}^{-3}$, the Phan *et al.* [4] event gives $E_\parallel \sim 1$, which is an order of magnitude larger than $E_\parallel \sim 0.08$ in 3D simulation. An upper limit on the rate of reconnection is yet to be established in the new 3D reconnection geometry as reconnection in narrower current layers may be more localized (few d_e's) in z than in the present 3D simulation. Additionally, the guide field of the Phan *et al.* [4] event was eight times larger than the guide field in our simulation, which could account for a much larger $E_\parallel$. Lastly, it is possible that reconnection embedded in fully developed turbulence [33–35] could produce conditions leading to an enhanced $E_\parallel$.

The spatial structure of the electric fields measured by MMS have significant differences from simulations, although both demonstrated highly spatially localized $E_\parallel$. The 2D and 3D simulations reconnected robustly for a duration $\sim 100\,\Omega_{ce}^{-1}$ (Fig. 1(b)) and both exhibit some localization of E_z in the inflow direction (Figs. 2(e) and (f)), however, not confined within the CS. Conversely, the Phan *et al.* [4] event exhibited a highly localized E_M (simulation E_z) along the normal direction (simulation $\hat{y}$), confined within the reconnection CS. Noting that the Phan *et al.* [4] event had a guide field eight times the reconnection field and given that such a large guide field may allow the reconnection structure to be confined to a much smaller spatial region, 3D simulations with such a large guide field may exhibit such localized E_M structure.

Simulating such a large guide field, especially with high plasma β, poses significant challenges for simulation because they require small time steps associated with high temperatures and long simulation domains along z.

Numerous numerical simulation studies have explored the interplay between reconnection and turbulence (e.g., [36–39]). In the MHD limit, magnetic field stochasticity in the form of 3D magnetic field wandering was shown to be essential for fast reconnection in turbulent fluid [33, 40, 41] and since this study has not been designed to study electron-only reconnection in self-consistently produced turbulence, the effects of stochasticity [28, 35, 42] is an important aspect that entails future examinations. Electron-only reconnection may play a key role in the dissipation of turbulent energy, but precisely how remains an active area of research. Since electron-only reconnection's prevalence has been observed at different regions [8, 9, 13, 43], investigating its basic properties at kinetic scales is relevant in understanding the interplay between reconnection and turbulence. The findings presented in this Letter demonstrate that 3D reconnection at electron scales is fundamentally different than the often studied 2D reconnection paradigm and indicate that 3D effects may alter energy dissipation channels at kinetic scales. Thus, extrapolations from 2D models to explore reconnection driven energy release in real systems must be taken with caution. How localized electron scale reconnection effects and controls large scale reconnection physics will require future investigations.

ACKNOWLEDGMENTS

This research was supported by NSF grants AGS-2024198, AGS-1602769, PHY1805829, NASA Grants 80NSSC21K1481, NNX17AI25G, 80NSSC20K0198, NNX16AF75G, 80NSSC19M0146, 80NNSC19K0848, 80NSSC18K0157, 80NSSC20K1781, and DOE Grant DE-SC0020294. We acknowledge high-performance computing support from Cheyenne [44] provided by NCAR's CISL, sponsored by the NSF. This research also used NERSC resources, a U.S. DOE office of Science User Facility operated under Contract No. DE-AC02-05CH11231.

[1] M. Yamada, R. Kulsrud, and H. Ji, Rev. Modern Phys. **82**, 603 (2010).

[2] T. Nagai, M. Fujimoto, Y. Saito, S. Machida, T. Terasawa, R. Nakamura, T. Yamamoto, T. Mukai, A. Nishida, and S. Kokubun, Journal of Geophysical Research: Space Physics **103**, 4419 (1998).

[3] V. Angelopoulos, J. P. McFadden, D. Larson, C. W. Carlson, S. B. Mende, H. Frey, T. Phan, D. G. Sibeck, K. Glassmeier, U. Auster, E. Donovan, I. R. Mann, I. J. Rae, C. T. Russell, A. Runov, X. Zhou, and L. Kepko, Science **321**, 931 (2008).

[4] T. D. Phan, J. P. Eastwood, M. A. Shay, J. F. Drake, B. U. Ö. Sonnerup, M. Fujimoto, P. A. Cassak, M. Øieroset, J. L. Burch, R. B. Torbert, A. C. Rager, J. C. Dorelli, D. J. Gershman, C. Pollock, P. S. Pyakurel, C. C. Haggerty, Y. Khotyaintsev, B. Lavraud, Y. Saito, M. Oka, R. E. Ergun, A. Retino, O. Le Contel, M. R. Argall, B. L. Giles, T. E. Moore, F. D. Wilder, R. J. Strangeway, C. T. Russell, P. A. Lindqvist, and W. Magnes, Nature **557**, 202 (2018).

[5] J. L. Burch, R. B. Torbert, T. D. Phan, L.-J. Chen, T. E. Moore, R. E. Ergun, J. P. Eastwood, D. J. Gershman, P. A. Cassak, M. R. Argall, S. Wang, M. Hesse, C. J. Pollock, B. L. Giles, R. Nakamura, B. H. Mauk, S. A. Fuselier, C. T. Russell, R. J. Strangeway, J. F. Drake, M. A. Shay, Y. V. Khotyaintsev, P.-A. Lindqvist, G. Marklund, F. D. Wilder, D. T. Young, K. Torkar, J. Goldstein, J. C. Dorelli, L. A. Avanov, M. Oka, D. N. Baker, A. N. Jaynes, K. A. Goodrich, I. J. Cohen, D. L. Turner, J. F. Fennell, J. B. Blake, J. Clemmons, M. Goldman, D. Newman, S. M. Petrinec, K. J. Trattner, B. Lavraud, P. H. Reiff, W. Baumjohann, W. Magnes, M. Steller, W. Lewis, Y. Saito, V. Coffey, and M. Chandler, Science **352**, aaf2939 (2016).

[6] F. D. Wilder, R. E. Ergun, S. Eriksson, T. D. Phan, J. L. Burch, N. Ahmadi, K. A. Goodrich, D. L. Newman, K. J. Trattner, R. B. Torbert, B. L. Giles, R. J. Strangeway, W. Magnes, P.-A. Lindqvist, and Y.-V. Khotyaintsev, Phys. Rev. Lett. **118**, 265101 (2017).

[7] S. Eriksson, F. D. Wilder, R. E. Ergun, S. J. Schwartz, P. A. Cassak, J. L. Burch, L.-J. Chen, R. B. Torbert, T. D. Phan, B. Lavraud, K. A. Goodrich, J. C. Holmes, J. E. Stawarz, A. P. Sturner, D. M. Malaspina, M. E. Usanova, K. J. Trattner, R. J. Strangeway, C. T. Russell, C. J. Pollock, B. L. Giles, M. Hesse, P.-A. Lindqvist, J. F. Drake, M. A. Shay, R. Nakamura, and G. T. Marklund, Phys. Rev. Lett. **117**, 015001 (2016).

[8] I. Gingell, S. J. Schwartz, J. P. Eastwood, J. L. Burch, R. E. Ergun, S. Fuselier, D. J. Gershman, B. L. Giles, Y. V. Khotyaintsev, B. Lavraud, P.-A. Lindqvist, W. R. Paterson, T. D. Phan, C. T. Russell, J. E. Stawarz, R. J. Strangeway, R. B. Torbert, and F. Wilder, Geophysical Research Letters **46**, 1177 (2019).

[9] S. Wang, L.-J. Chen, N. Bessho, M. Hesse, L. B. Wilson III, B. Giles, T. E. Moore, C. T. Russell, R. B. Torbert, and J. L. Burch, Geophysical Research Letters **46**, 562 (2019).

[10] M. E. Mandt, R. E. Denton, and J. F. Drake, Geophys. Res. Lett. **21**, 73 (1994).

[11] P. Sharma Pyakurel, M. A. Shay, T. D. Phan, W. H. Matthaeus, J. F. Drake, J. M. TenBarge, C. C. Haggerty, K. G. Klein, P. A. Cassak, T. N. Parashar, M. Swisdak, and A. Chasapis, Physics of Plasmas **26**, 082307 (2019), https://doi.org/10.1063/1.5090403.

[12] J.-S. He, E. Marsch, C.-Y. Tu, Q.-G. Zong, S. Yao, and H. Tian, Journal of Geophysical Research: Space Physics **116**, A06207 (2011).

[13] J. E. Stawarz, J. P. Eastwood, T. D. Phan, I. L. Gingell,

M. A. Shay, J. L. Burch, R. E. Ergun, B. L. Giles, D. J. Gershman, O. L. Contel, P.-A. Lindqvist, C. T. Russell, R. J. Strangeway, R. B. Torbert, M. R. Argall, D. Fischer, W. Magnes, and L. Franci, The Astrophysical Journal **877**, L37 (2019).
[14] N. Bessho, L.-J. Chen, S. Wang, M. Hesse, and L. B. Wilson III, Geophysical Research Letters **46**, 9352 (2019).
[15] W. H. Matthaeus and S. L. Lamkin, Physics of Fluids **29**, 2513 (1986).
[16] A. Retinò, D. Sundkvist, A. Vaivads, F. Mozer, M. André, and C. J. Owen, Nature Physics **3**, 236 (2007).
[17] S. Servidio, W. H. Matthaeus, M. A. Shay, P. A. Cassak, and P. Dmitruk, Phys. Rev. Letters **102**, 115003 (2009).
[18] S. Boldyrev and N. F. Loureiro, Phys. Rev. Research **1**, 012006 (2019).
[19] N. F. Loureiro and S. Boldyrev, The Astrophysical Journal **890**, 55 (2020), arXiv:1907.09610 [physics.plasm-ph].
[20] A. Zeiler, D. Biskamp, J. F. Drake, B. N. Rogers, M. A. Shay, and M. Scholer, J. Geophys. Res. **107**, 1230 (2002), doi:10.1029/2001JA000287.
[21] J. D. Huba and L. I. Rudakov, Phys. Plasmas **9**, 4435 (2002).
[22] M. A. Shay, J. F. Drake, M. Swisdak, W. Dorland, and B. N. Rogers, Geophys. Res. Lett. **30**, 1345, doi:10.1029/2002GL016267 (2003).
[23] N. Jain, A. S. Sharma, L. M. Zelenyi, and H. V. Malova, Annales Geophysicae **30**, 661 (2012).
[24] N. Jain, J. Büchner, S. Dorfman, H. Ji, and A. Surjalal Sharma, Physics of Plasmas **20**, 112101 (2013), https://doi.org/10.1063/1.4827828.
[25] T. K. M. Nakamura, R. Nakamura, A. Alexandrova, Y. Kubota, and T. Nagai, Journal of Geophysical Research: Space Physics **117** (2012), https://doi.org/10.1029/2011JA017006.
[26] L. S. Shepherd and P. A. Cassak, Journal of Geophysical Research: Space Physics **117** (2012), 10.1029/2012JA017867.
[27] T. C. Li, Y.-H. Liu, M. Hesse, and Y. Zou, Journal of Geophysical Research: Space Physics **n/a**, e2019JA027094 (2020), e2019JA027094 2019JA027094.
[28] G. Kowal, A. Lazarian, E. T. Vishniac, and K. Otmianowska-Mazur, Astrophys. J. **700**, 63 (2009), arXiv:0903.2052 [astro-ph.GA].
[29] Y.-H. Liu, T. C. Li, M. Hesse, W. J. Sun, J. Liu, J. Burch, J. A. Slavin, and K. Huang, Journal of Geophysical Research: Space Physics **124**, 2819 (2019).
[30] K. Huang, Y.-H. Liu, Q. Lu, and M. Hesse, Geophysical Research Letters **47**, e2020GL088147 (2020).
[31] J. C. Meyer, *Structure of the diffusion region in three dimensional magnetic reconnection*, Ph.D. thesis, University of Delaware (2015).
[32] S. Dorfman, H. Ji, M. Yamada, J. Yoo, E. Lawrence, C. Myers, and T. D. Tharp, Geophysical Research Letters **40**, 233 (2013).
[33] A. Lazarian and E. Vishniac, Ap. J. **517**, 700 (1999).
[34] A. Lazarian, G. Kowal, E. Vishniac, K. Kulpa-Dubel, and K. Otmianowska-Mazur, Highlights of Astronomy **15**, 434 (2010).
[35] A. Lazarian, G. L. Eyink, A. Jafari, G. Kowal, H. Li, S. Xu, and E. T. Vishniac, Physics of Plasmas **27**, 012305 (2020), arXiv:2001.00868 [astro-ph.HE].
[36] S. S. Cerri and F. Califano, New Journal of Physics **19**, 025007 (2017).
[37] A. Mallet, A. A. Schekochihin, and B. D. G. Chandran, Monthly Notices of the Royal Astronomical Society **468**, 4862 (2017), arXiv:1612.07604 [astro-ph.SR].
[38] F. Califano, S. S. Cerri, M. Faganello, D. Laveder, and M. W. Kunz, ArXiv e-prints (2018), arXiv:1810.03957 [physics.plasm-ph].
[39] S. Adhikari, M. A. Shay, T. N. Parashar, P. S. Pyakurel, W. H. Matthaeus, D. Godzieba, J. E. Stawarz, J. P. Eastwood, and J. T. Dahlin, Physics of Plasmas **27**, 042305 (2020), https://doi.org/10.1063/1.5128376.
[40] G. L. Eyink, A. Lazarian, and E. T. Vishniac, Astrophys. J. **743**, 51 (2011), arXiv:1103.1882 [astro-ph.GA].
[41] G. Eyink, E. Vishniac, C. Lalescu, H. Aluie, K. Kanov, K. Bürger, R. Burns, C. Meneveau, and A. Szalay, Nature (London) **497**, 466 (2013).
[42] G. Kowal, D. A. Falceta-Gonçalves, A. Lazarian, and E. T. Vishniac, Astrophys. J. **892**, 50 (2020), arXiv:1909.09179 [astro-ph.HE].
[43] M. Hubbert, Y. Qi, C. T. Russell, J. L. Burch, B. L. Giles, and T. E. Moore, Geophysical Research Letters **48**, e2020GL091364 (2021), e2020GL091364 2020GL091364.
[44] Computational and Information Systems Laboratory, “Cheyenne: HPE/SGI ICE XA System (University Community Computing),” (2017).